

Mechanism of Membrane Poration by Shock Wave Induced Nanobubble Collapse: A Molecular Dynamics Study

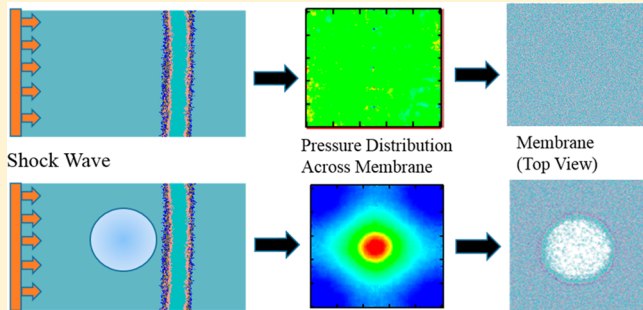
Upendra Adhikari,[†] Ardeshir Goliae,[‡] and Max L. Berkowitz*,[†]

[†]Department of Chemistry, University of North Carolina at Chapel Hill, Chapel Hill, North Carolina 27599, United States

[‡]Department of Biochemistry and Biophysics and Program in Molecular and Cellular Biophysics, University of North Carolina at Chapel Hill, Chapel Hill, North Carolina 27599, United States

Supporting Information

ABSTRACT: We performed coarse-grained molecular dynamics simulations in order to understand the mechanism of membrane poration by shock wave induced nanobubble collapse. Pressure profiles obtained from the simulations show that the shock wave initially hits the membrane and is followed by a nanojet produced by the nanobubble collapse. While in the absence of the nanobubble, the shock wave with an impulse of up to 18 mPa s does not create a pore in the membrane, in the presence of a nanobubble even a smaller impulse leads to the poration of the membrane. Two-dimensional pressure maps depicting the pressure distributed over the lateral area of the membrane reveal the differences between these two cases. In the absence of a nanobubble, shock pressure is evenly distributed along the lateral area of the membrane, while in the presence of a nanobubble an unequal distribution of pressure on the membrane is created, leading to the membrane poration. The size of the pore formed depends on both shock wave velocity and shock wave duration. The results obtained here show that these two properties can be tuned to make pores of various sizes.



INTRODUCTION

The interaction of shock waves with biological cells is a subject of active research.^{1–7} This interaction can produce both positive and negative effects: controlled shock waves have a potential for medical use, since they increase the permeability of cell membranes⁸ and this allows various macromolecules, such as drugs and also genetic material to enter the cell.^{9–17} On the negative side uncontrolled shock waves produced during a blast may damage brain cells, thus causing blast induced traumatic brain injury (bTBI) and neural cell damage or even its death. To understand the details and the role of shock waves in bTBI, experiments^{4,18–20} using shock tubes and also computer simulations^{5,21} have been performed. However, the mechanisms behind the bTBI, especially mild TBI (mTBI) are still not clearly understood, as the severity of TBI depends on several factors, such as shock wave amplitude, duration of exposure, distance from the blast, etc.

The effect of shock waves on biomembranes can be enhanced by the collapse of bubbles present in the vicinity of these membranes.^{12,13,22–25} Thus, ultrasound induced collapse of microbubbles is found to be responsible for the permanent poration of cell membranes^{12,26–29} due to the formation of a fluid jet as a result of a bubble collapse. Not only the collapse of microbubbles, but also of nanobubbles is considered to have a potential to produce substantial pores in a cell membrane due to a shock wave impact.^{1,5,30} Although there was some debate

about the existence of nanobubbles in the past, recent research suggests their viability.^{31–36}

Detailed information about the process of nanobubble collapse due to an impinging shock wave and the resulting damage to a biomembrane can be obtained from molecular simulations. Recently Choubey et al.¹ observed in their all-atom molecular dynamics (MD) simulations a shock wave induced nanobubble collapse that formed a nanojet. This nanojet had a high velocity and moved toward the membrane, creating a nanopore in it, thus allowing permeation of water and other bigger molecules across the membrane. Our group also investigated recently^{5,30} the effect of shock wave induced collapse of a single and also multiple nanobubbles by using coarse-grained (CG) MD simulations. The results from our CG MD simulations were in a nice agreement with the all-atom simulations performed by Choubey et al.¹ Although, as we observed, the pores often recovered, some lipids from membranes were expelled out of the bilayer, even forming micelles in some cases, depending on the shock velocities. Also, as we observed, the damage to the membrane depended on the size of the nanobubbles. For instance, the collapse of a nanobubble of a diameter $D = 40$ nm produced a bigger pore and it took a longer time for the membrane to recover,

Received: March 6, 2015

Revised: April 22, 2015

Published: April 23, 2015

compared to the case when a nanobubble of a diameter $D = 20$ nm collapsed. We also studied the effect on the membrane when multiple nanobubbles, positioned in different arrangements, collapsed under the impinging shock wave³⁰ and observed that more damage to the membrane was done when two nanobubbles were placed in a serial arrangement with respect to each other, compared to cases when nanobubbles were placed in other configurations, like parallel and/or slanted.

The previous work that studied the effect of shock waves, but in the bubble absence, demonstrated that the peak pressure and the duration of the membrane exposure to the shock wave are major contributing factors that determine the degree of cell membrane damage. It was determined in that work that when the shock wave impinges on the membrane, it is the pressure impulse, rather than the peak value of the pressure, that is usually considered.^{2,3,29} The impulse (I) is defined as the time integral over shock wave pressure profile:

$$I = \int_0^{t^+} P(t) dt \quad (1)$$

where $P(t)$ is the shock wave pressure and t^+ is the time duration of the positive phase of the shock wave.² It was also observed^{2,8} that when the impulse was above a certain value, the cell membrane as a whole became severely damaged, resulting in a cell death. In the presence of bubbles, a bubble collapse produces a nanojet that causes a localized damage to the membrane by creating small pores in it. Can an impulse, defined above, still be a measure of the possible damage produced by shock waves to membranes when a bubble is present? There are some other questions related to the understanding of a nanobubble collapse induced membrane poration that still require answers. For example, why a shock wave of certain impulse and shock velocity does not form a pore in the membrane, whereas a nanojet formed by a nanobubble collapse produces one? What are the major differences in the shock wave impact in the presence and absence of nanobubbles in the vicinity of the membrane?

This kind of questions probably may be answered by carefully observing mechanistic details of the events, specifically pressure distributions at various stages of shock wave induced nanobubble collapse and nanojets hitting the membrane. Therefore, in this paper we present the results from MD simulations we performed to get an insight into the pressure behavior when shock waves hit nanobubbles next to lipid bilayers that model cell membranes. In our simulations nanobubbles (diameter $D = 60$ nm) are induced to collapse via shock wave propagating toward the bilayer membrane. Different impulses of shock wave and various particle velocities are chosen to create various magnitudes of damage to the membrane. Pressure distribution at the membrane position is calculated at various stages of shock wave simulation, both in the presence and absence of the nanobubble. Nanobubble with a diameter $D = 20$ nm is also considered for a comparison purpose. We observe that 2-dimensional pressure distributions obtained at the membrane position accurately reflect the difference between the shockwave impact in the presence and in the absence of nanobubbles. We also studied what happens when a nanobubble collapses without the presence of a shock wave and the effects observed in this case are compared with the effects produced in the presence of shock waves.

METHODS

All computer simulations were performed using Gromacs 4.6.6 package,^{37–40} except that the pressure calculation was done using Gromacs-4.0.2_local pressure⁴¹ version of Gromacs. We described the interactions by the CG MARTINI^{42,43} force field, since it is widely and often successfully used in biomolecular simulations of systems containing lipid membranes.^{44,45} Our membrane was modeled by a lipid model bilayer consisting of dipalmitoylphosphatidyl choline (DPPC) lipids. The lipid bilayer contained 32 768 DPPC CG molecules and it was constructed by replicating a small bilayer containing 128 DPPC molecules 16 times in x and y directions. After energy minimization of the bilayer, it was solvated by 11 444 725 (~11.5 million) nonpolarizable CG water molecules. This system containing water and lipids was energy minimized and equilibrated in the isothermal–isobaric (NPT) ensemble for 20 ns at temperature of 323 K and pressure of 1 bar under semi-isotropic conditions. The time step in the equilibration run was 30 fs, and Berendsen's scheme⁴⁶ was used to keep constant temperature and pressure. The time constants for temperature and pressure couplings were equal to 0.3 and 3 ps respectively, and compressibility was 3×10^{-5} bar. Nonbonded interactions were cut off at 1.2 nm using the shift scheme. The size of the system after equilibration was $101.1 \times 103.4 \times 137.5$ nm in x , y and z directions, respectively, with the membrane positioned in parallel to the xy plane at $z \approx 90$ nm.

Shock wave simulations were performed on this equilibrated system with added spherical nanobubbles that were created by removing water molecules from the inside of the bubble (i.e., actually creating a void). The shock waves were generated by using the momentum mirror protocol applied in this kind of simulations in the past.^{1,47,48} In this protocol all particles move with velocity v_p toward the mirror placed at the end of the box in the $-z$ direction; they get reflected upon impact, thus creating a shock wave moving with velocity greater than v_p in the $+z$ direction. This procedure in effect is equivalent to having a massive piston moving toward the $+z$ direction with velocity v_p and reflecting all the particles coming in contact with it, thus creating a shock wave. Periodic boundary conditions (PBC) were applied only in the x and y directions and not in the z direction. A 2 nm vacuum layer was added at the end of the system along the z direction, so that the particles would not overlap and collide with the mirror at the very beginning of the simulation. To mimic the propagation of smaller by value shock pulses, the piston was stopped after a short time and the shock wave formed was allowed to continue with its motion in the $+z$ direction. Various piston stop times were chosen to create shock waves of various impulses. All shock simulations were performed in constant energy ensemble and the cutoff value for interactions was 1.4 nm instead of the usual 1.2 nm for better energy conservation. The neighbor list was updated every 5 steps, instead of the usual 10. The time step in the shock simulations was 4 fs. The shock velocity was calculated by identifying the discontinuity in density along the $+z$ direction. Pressure was calculated by using the method developed by Ollila et al.⁴¹ and was obtained by discretizing the system into small cubes of dimensions 0.5 nm. The time intervals reported here are actual simulation times and not the equivalent times often reported for simulations with MARTINI. Figures were created using the VMD program.⁴⁹

For a given choice of a piston velocity or stoppage time, presence or absence of a bubble, we performed a number of

Table 1. Summary of the Results from Shock Wave Simulations

bubble diameter, nm	v_p (km/s)	τ_s (ps)	total I (mPa s)	velocity ^a of the shock wave (km/s)	maximum velocity of the nanojet (km/s)	maximum radius of the pore formed (nm)
60	1.0	3	5.45	2.16	2.06	15.3
60	1.0	5	14.93	2.55	3.38	20.5
60	0.5	5	3.00	1.87	1.06	no pore
60	0.5	10	5.49	2.21	2.48	15.5
20	1.0	3	7.18	2.16	2.75	5.3
0	1.0	3	8.96	2.16	—	no pore
0	1.0	5	17.57	2.55	—	no pore

^aVelocity of shock wave at the time when it hits the membrane.

simulations that differed from each other by a choice of the initial conditions. In all simulations with the same parameters, but different initial conditions, the results looked very similar and therefore we report here the results from one of each of the simulations of certain type. The types of the systems we discuss in this paper are summarized in Table I

RESULTS

As stated in the Methods, shock waves were created using the momentum mirror approach, a diagrammatic sketch of which is shown in Figure 1. Once the particles hit the piston with

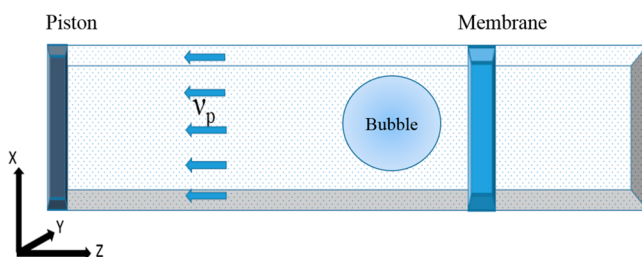


Figure 1. Representation of systems simulated in this work. We also simulated a system that did not contain a bubble and a system where a shock wave was not created.

velocity v_p (particle velocity), they are reflected and create a region of higher density that moves with a higher velocity v_s (shock wave velocity). After a short time (denoted by " τ_s " here) we stopped the piston, but the shock wave continued to propagate in the $+z$ direction. Such shock wave propagation can be clearly seen in the panels shown in Figure 2, depicting the 2-dimensional water density plots. At the beginning of the shock wave propagation, at $t = 0$ ps, the shocked region at the extreme

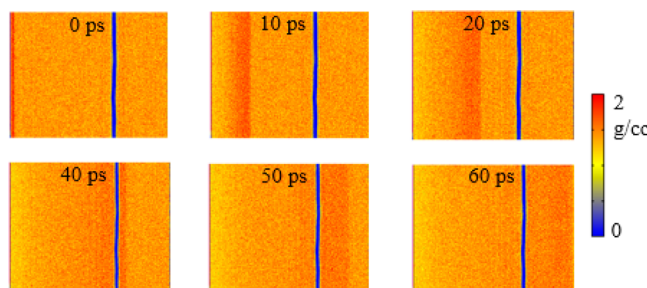


Figure 2. 2-Dimensional water density maps showing the propagation of the shock wave in a system without a bubble at various stages of simulations. In this case the piston stopped at 3 ps ($\tau_s = 3$ ps), and $v_p = 1.0$ km/s. The density decreases is coded in change of color from red to blue.

left is depicted in bright red. The propagation of the shock region with time is clearly seen in the panels, since the bright red region moves in the $+z$ direction. As the shock wave continues to propagate, both its intensity and velocity decrease. For completeness and comparison of the density profiles of water when the shock wave propagates in the systems with and without the bubble we show in Figure 3 the 2-dimensional water density plots in the presence of the nanobubble. More details about these density plots and water jet properties when the bubble collapses, can be found in the previous work.⁵ In this work we concentrate on the study of pressure profiles in the membrane region.

By stopping the piston at various times, shock waves with various impulses can be created. Similarly, one can vary particle velocities to change the shock wave impulses. Below we report results from simulations using different values of v_p , different τ_s and also different values of the nanobubble diameter. To understand the role of the bubble we also simulated a system with no bubble present.

Shock Wave Simulations with Particle Velocity (v_p) = 1.0 km/s. Here we discuss the results from simulations with $v_p = 1.0$ km/s. To see how the piston stop time influences these results, we performed simulations with $\tau_s = 3$ ps, and 5 ps. Because the shock wave is moving in the z -direction, we calculated the change of the normal pressure component, P_{zz} , and since we are interested in the properties of the membrane, we measured the pressure at the membrane position and studied it as a function of time.

(a). *Simulations with $\tau_s = 3$ ps.* The change in average normal pressure across membrane surface (the pressure profile) for simulation with $\tau_s = 3$ ps of a system without a bubble is shown in Figure 4. This pressure profile displays the classical Friedlander curve seen for shock waves. According to Friedlander profile, as the shock wave arrives, there is a sharp rise in pressure (positive phase) followed by a very rapid decrease of pressure, which reaches a minimum at a negative value, and then the pressure rises again toward the normal pressure. The pressure value remains at 1 bar until the shock wave arrives. Upon the shock wave arrival, the pressure rises very sharply up to a value of 478 MPa (at ~ 40 ps of the simulation time), then it gradually decreases, becoming negative and reaches the peak negative pressure value (-76 MPa) at ~ 104 ps. As in the Friedlander curve, the pressure returns to normal, and in our simulation it happens at time ~ 128 ps. Although the pressure peak value is very high, the duration of the shock impulse is very short and therefore the value of the impulse I from eq 1 in our simulation is only 8.96 mPa s. This value is much smaller than the experimentally measured² value of an impulse of 54 Pa s, that caused only an uptake of calcein molecules into the cell, but not the cell death.

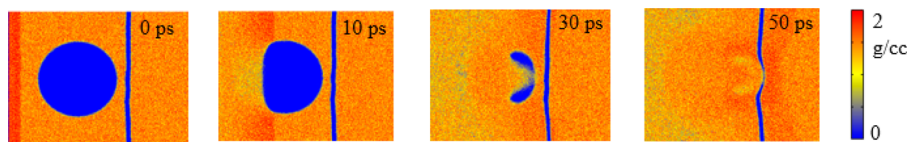


Figure 3. 2-Dimensional water density maps showing the collapse of a nanobubble after the shock wave ($\tau_s = 5$ ps and $v_p = 1.0$ km/s) passage. Only a slice of 20 nm in width is considered (from $X = 40$ nm to $X = 60$ nm) for a better view of the bubble collapse.

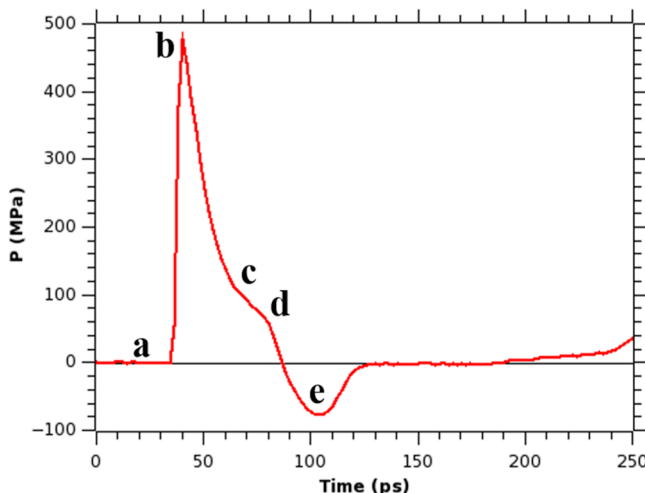


Figure 4. Time dependence of the pressure normal to the membrane surface (pressure profile at the membrane position) when $v_p = 1.0$ km/s and $\tau_s = 3$ ps in a system containing no bubble. The letters (a–e) correspond to different stages of the shock wave propagation.

Therefore, we should not expect that a major damage to the membrane occurs when a shock wave with an impulse of 8.96 mPa s hits a cell membrane. A two-dimensional diagram showing the pressure across the x and y axes of the membrane helps to understand how the distribution of normal pressure changes as the shock wave passes through the lipid bilayer, and

this diagram is depicted in Figure 5. Notice that the average pressure calculated from the 2-d map at a certain time corresponds to a value of the pressure from Figure 4 at that particular time. For instance, the average pressure of Figure 5b is equal to 478 MPa corresponding to the value of pressure at point "b" in Figure 4. As we can see from Figure 5, for a system containing just water and the bilayer and exposed to a shock, the pressure is distributed homogeneously along the surface of the bilayer and the values of the pressure fluctuations are very small. Thus, as the shock arrives at the membrane, the entire bilayer is experiencing the same pressure with forces pointing in the same direction. The snapshots of the bilayer membrane at various shock simulation times are shown in Figure S1 of the Supporting Information. As this figure shows, even when a shock wave hits the membrane with an impulse of 8.96 mPa s and a peak pressure of 478 MPa, the membrane remains intact. Although no pore formation was observed, the bilayer has undergone slight compression as the shock wave reached the membrane at 40 ps, but it returned to an original shape after the shock wave passed through, as can be seen from Figure S1.

A completely different scenario is observed when a nanobubble is present in the vicinity of the membrane. In our simulations of systems containing a nanobubble with a diameter $D = 60$ nm, the bubble was placed at a distance about 3 nm away from the membrane and its center coincided with the membrane center in x and y directions. As the shock wave propagated toward the membrane, it initially impinged on the nanobubble and after some period of time hit the bilayer. The

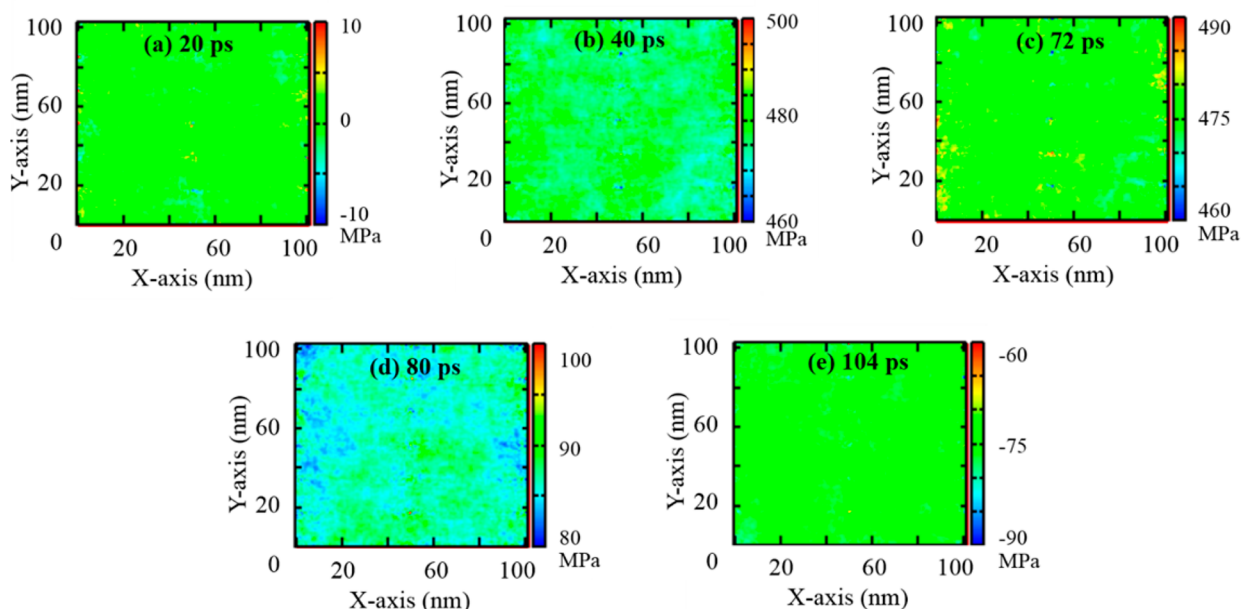


Figure 5. 2-Dimensional pressure maps at the membrane position at various times with $v_p = 1.0$ km/s and $\tau_s = 3$ ps in a simulation containing no bubble. The letters a–e correspond to the same stages as in Figure 4.

shock wave induced nanobubble collapse produced a nanojet of water particles moving with high velocity, and this nanojet moved in the same direction as the shock wave. The profile of the membrane pressure (for simulation with $\tau_s = 3$ ps) in the presence of the nanobubble is shown in Figure 6. Several

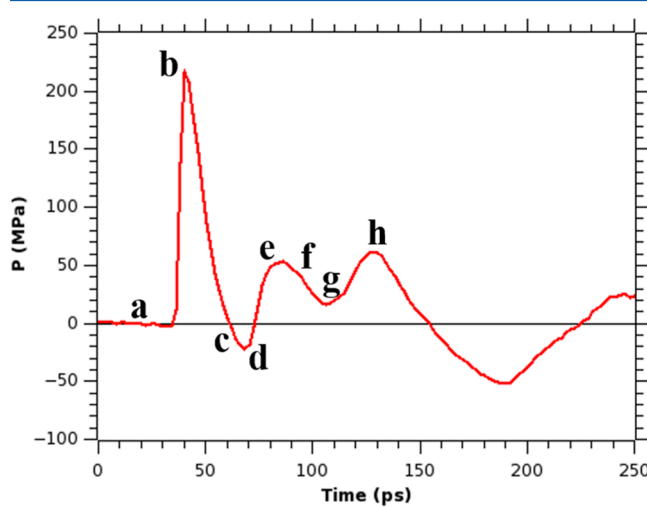


Figure 6. Pressure profile at the membrane when $v_p = 1.0 \text{ km/s}$ and $\tau_s = 3 \text{ ps}$ in a system containing a bubble with $D = 60 \text{ nm}$. The letters a–h correspond to different stages of the shock wave propagation.

differences can be seen between the profiles from Figure 4 (simulation without a bubble) and Figure 6 (simulation with a bubble). Although the shock wave hits the membrane at the same time (~ 40 ps), the peak pressure (~ 217 MPa) and the impulse due to the shock wave (2.52 mPa s) measured as an integral over pressure values in the first positive region in Figure 6 are smaller in the latter case. These smaller values are due to the presence of the bubble that hinders the shock wave propagation. Another clear difference in this pressure profile can be seen in the behavior of the pressure, after the shock wave pressure enters its negative phase. Unlike in the case of the bubble absence, after the shock wave entered its negative phase, the pressure started to rise toward high positive values reaching a value of ~ 50 MPa delivering an additional 2.93 mPa

s of positive impulse. The second peak in pressure is due to the pressure created by the nanobubble collapse. Despite the deliverance of a smaller total positive impulse and that the peak pressure initially had a smaller value in case when the nanobubble was present, we observed that the collapse of a nanobubble resulted in a formation of a pore in the membrane.

To understand why poration occurred we again looked at the distribution of the pressure on the membrane surface. Since the nanobubble is located next to the membrane center along x and y axes we expected to see a high pressure region at the center of the membrane after the nanobubble collapses into it. Indeed, the 2-dimensional pressure maps at various simulation times, shown in Figure 7, display an interesting pattern of pressure distribution along the x and y axes. Before the shock wave hits the membrane (Figure 7a), the pressure is close to 0 MPa, just like in the system without a nanobubble. But as the shock wave hits the membrane, the pressure distribution map looks distinctly different from the map for the system without a bubble. At 40 ps (Figure 7b), which is the time when the membrane experiences the peak pressure, the pressure is lower at the center (blue color), whereas it is higher (~ 300 MPa) in the surrounding of the small circular central region. The lower pressure region at the center is due to the presence of the bubble in front of it, which hinders the initial shock wave and also lowers the average peak pressure. As the simulation progresses, the shock wave passes the membrane and the negative pressure phase starts to build-up at the membrane at about 60 ps. At the time when the negative pressure is building up, the nanobubble collapses, producing a high-pressure region at the center of the membrane. So, at the same time when the negative pressure is building up in other region of the membrane, a positive pressure build up takes place at the center of the membrane. Figure 7 shows that as time progresses from 60 to 70 ps of the simulation, the difference in pressure between the central higher pressure region (red) and lower pressure region (blue) increases. This unequal pressure distribution persists and increases in time up to 80 ps, and it is responsible for the poration of the membrane, since it produces forces acting on the membrane in different directions. After the nanojet passes through, the pressures gradually decrease and their distribution becomes homogeneous again

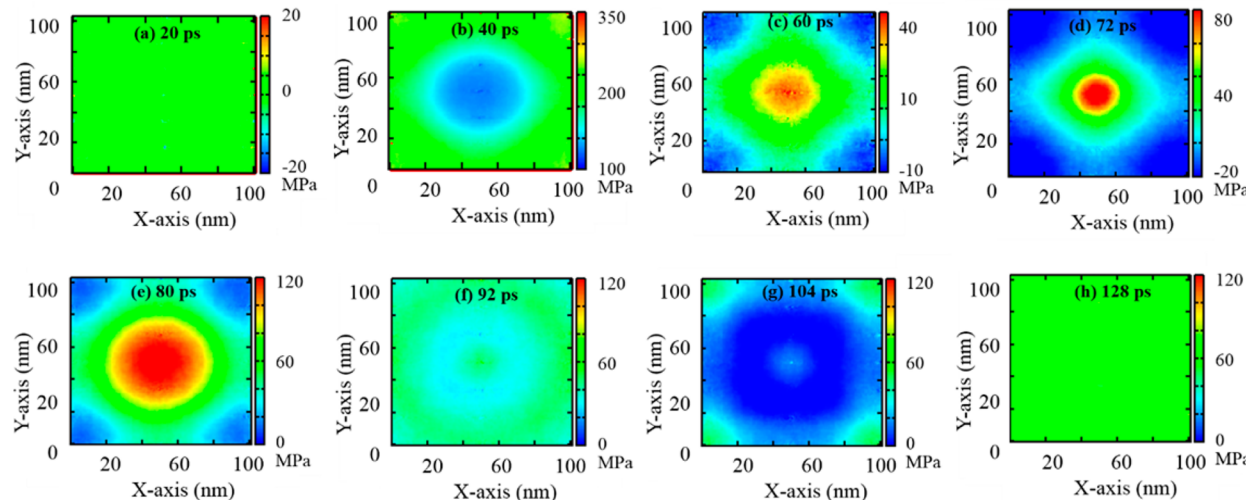


Figure 7. 2-Dimensional pressure maps at the membrane position at various times with $v_p = 1.0 \text{ km/s}$ and $\tau_s = 3 \text{ ps}$ in a simulation containing a bubble ($D = 60 \text{ nm}$). The letters a–h correspond to the same stages as in Figure 6

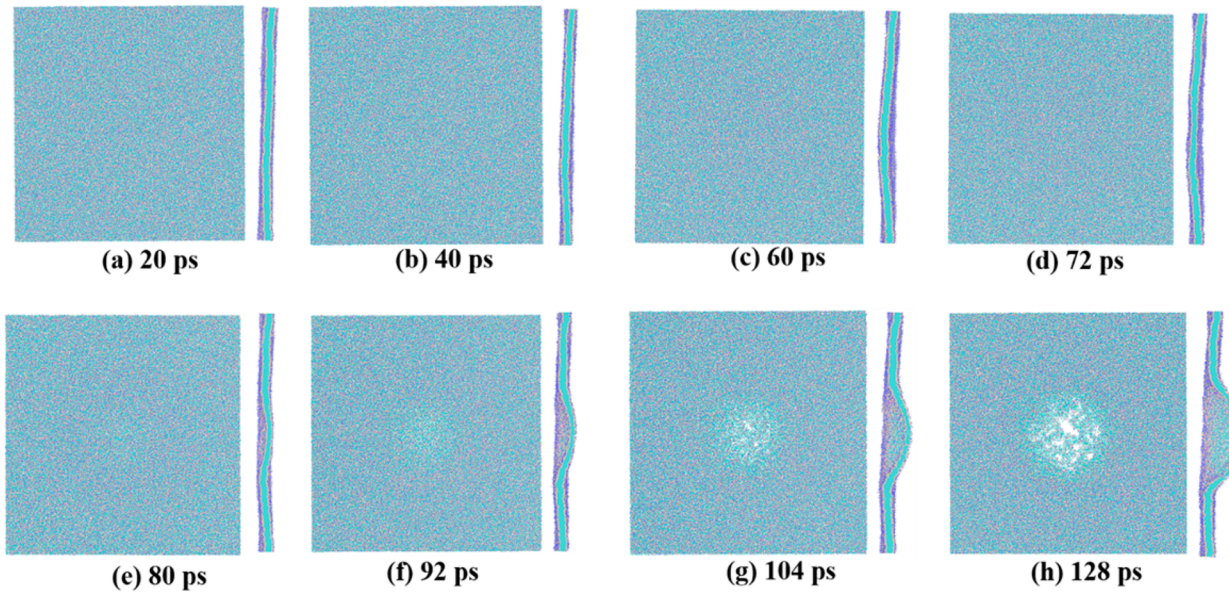


Figure 8. Snapshots of the bilayer membrane at various times of the simulations without a bubble when $\nu_p = 1.0 \text{ km/s}$ and $\tau_s = 3 \text{ ps}$ and $D = 60 \text{ nm}$. The view from the top is on the left and the side view is on the right.

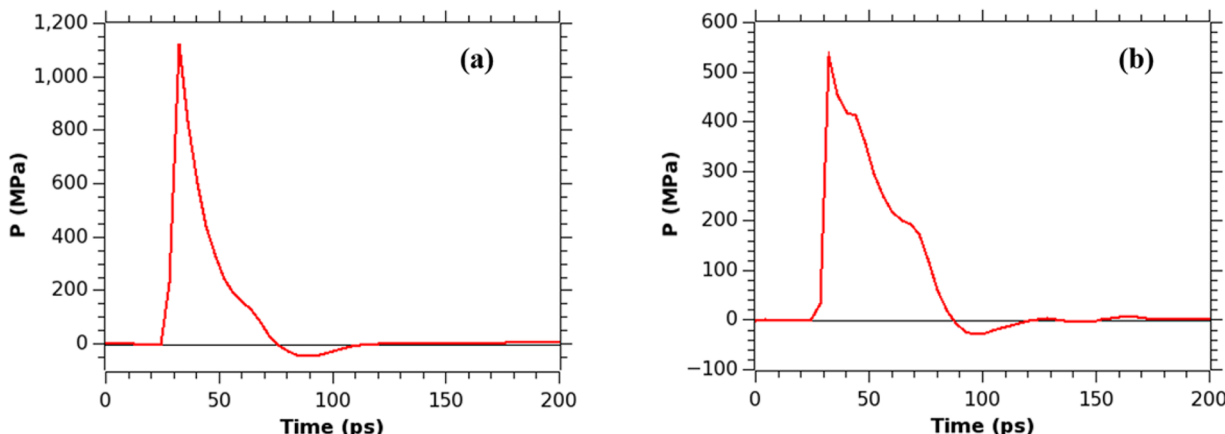


Figure 9. Pressure profiles at the membrane position in simulations with $\nu_p = 1.0 \text{ km/s}$, $\tau_s = 5 \text{ ps}$, (a) when there is no bubble is present or (b) when there is a nanobubble present ($D = 60 \text{ nm}$).

(Figure 7h). The snapshots of the membrane for this simulation are shown in Figure 8. We observe that as the difference in pressure values builds up at the membrane, the pore formation starts ($\sim 80 \text{ ps}$, see Figure 8e) and a bigger pore can be observed at $\sim 128 \text{ ps}$ of the simulation time (Figure 8h).

(b). $\tau_s = 5 \text{ ps}$. As expected, similar results are obtained when the piston is stopped after 5 ps of its motion, instead of 3 ps, but the effects of the shock wave impact are much more pronounced in this case. The pressure profiles at the membrane for $\tau_s = 5 \text{ ps}$ are given in Figures 9a and 9b. Figure 9a represents the pressure profile for the system with no bubble. The shock wave hits the membrane at 32 ps, slightly earlier than in case when $\tau_s = 3 \text{ ps}$, and the peak pressure reaches a value of 1126 MPa, which is more than twice the value of pressure reached in the simulation with $\tau_s = 3 \text{ ps}$. The positive phase impulse is 17.57 mPa s. The negative phase also starts earlier, at about 78 ps. No pore formation is observed even when transferring this impulse. Just like in case of $\tau_s = 3 \text{ ps}$, the pressure distribution map shows an equal pressure distribution along the x and y axes of the membrane. The pressure distribution maps and

snapshots of the membrane at various simulation times are given in Figures S2 and S3 of the Supporting Information.

Figure 9b displays the pressure profile for the system with a nanobubble. In this case, after the shock wave hits the membrane at 32 ps, the pressure stays positive for a longer time duration. Moreover, the figure shows the presence of two shoulders in the main peak, which are due to the nanobubble collapse. Unlike in case with $\tau_s = 3 \text{ ps}$, where two separate peaks were observed due to shock wave and nanojet, in $\tau_s = 5 \text{ ps}$ case the nanojet pressure peak hits almost immediately after the shock wave has passed. This is not surprising given the velocity of the shock wave, so that nanojet moves much faster than in case with $\tau_s = 3 \text{ ps}$. The total positive impulse is 14.93 mPa s and the peak pressure is 533 MPa. The pressure distribution map is similar to that of the map in case $\tau_s = 3 \text{ ps}$, but the difference in values for the higher (red at the center) and lower (blue) pressure regions is much larger in this case. This bigger inequality in pressure results in the formation of a larger sized pore and more damage to the membrane. The 2-dimensional pressure maps and snapshots of the membrane at various

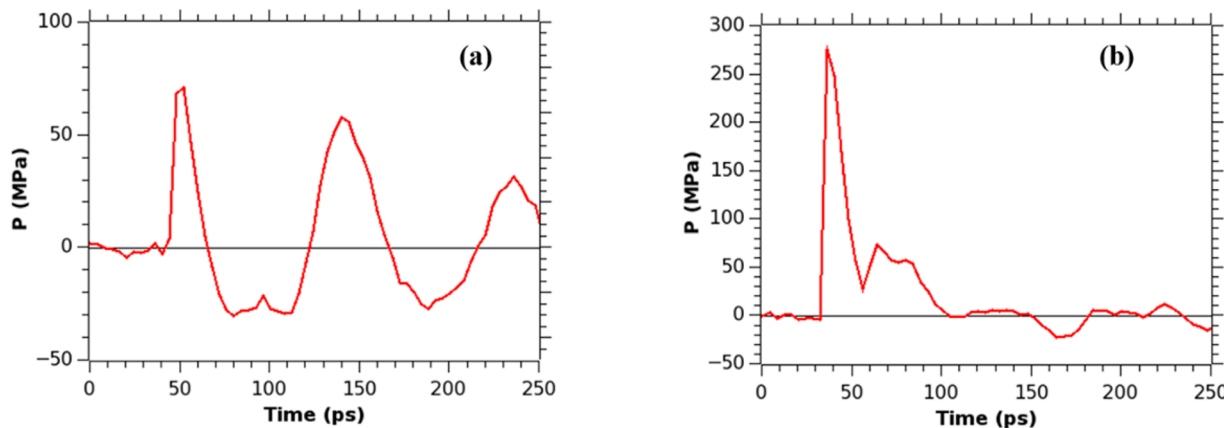


Figure 10. Pressure profiles at the membrane position in simulations with $\nu_p = 0.5$ km/s. (a) $\tau_s = 5$ ps and (b) $\tau_s = 10$ ps; in both cases a nanobubble is present ($D = 60$ nm).

simulation times are presented in the Supporting Information, Figures S4 and S5, respectively.

Shock Wave Simulations with Particle Velocity (ν_p) = 0.5 km/s. Two piston stopping times ($\tau_s = 5$ and 10 ps) were chosen for the simulations with 0.5 km/s particle velocity. The pressure profiles obtained at these conditions are shown in Figure 10. As the particle velocity is smaller than in the previously described cases, the shock wave velocity also becomes smaller. Because of this reason the shock wave arrives at the membrane later and the peak pressure is smaller as well.

When $\tau_s = 5$ ps, the shock wave arrives at the membrane at about 48 ps. The peak pressure is just 71 MPa and the total positive impulse is 2.27 mPa s. These values are around five times smaller than in case when $\nu_p = 1.0$ km/s. The pressure wave generated by the nanojet reaches the membrane at 124 ps. The 2-d pressure maps and the snapshots of the membrane at various times are given in Supporting Information, Figures S6 and S7, respectively. As we can see from Figure S6, when the nanojet arrives at the membrane and hits it, the pressure at the center of the membrane becomes bigger and decreases as we go away from the center, just like in case when $\nu_p = 1.0$ km/s. But the unequal distribution of the high and the low pressure regions is substantially smaller (maximum 30 MPa), and as a result no pore formation in the membrane occurs. If $\tau_s = 10$ ps, the shock wave arrives at the membrane at 36 ps, slightly earlier than when $\tau_s = 5$ ps. The peak pressure rises up to 276 MPa and the total impulse is 5.49 mPa s. These values are close to the corresponding ones from simulations with $\nu_p = 1.0$ km/s and $\tau_s = 3$ ps. The normal pressure distribution along x and y axis at the membrane and size of the pore formed also resemble that of $\nu_p = 1.0$ km/s and $\tau_s = 3$ ps (as shown in Table 1). The pressure maps and snapshots of the membrane at various simulation times are provided in Supporting Information, Figures S8 and S9, respectively. Thus, our simulations show that one can vary either the particle velocity or the time of the piston motion creating the shock wave to produce same result.

Shock Wave Simulations with a Smaller Nanobubble (Diameter, $D = 20$ nm). A system having a smaller nanobubble ($D = 20$ nm) was also considered for the comparison purposes. Particle velocities of 1.0 km/s, and $\tau_s = 3$ ps were chosen in this case. The pressure profile for this system is shown in Figure 11. The peak pressure (~348 MPa) and the total impulse (7.19 mPa s) of the shock wave hitting the membrane are slightly larger than in the case of 60 nm bubble due to lesser hindrance posed by the smaller bubble.

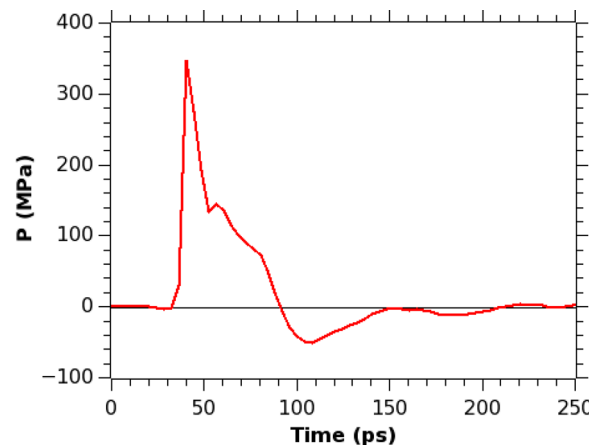


Figure 11. Pressure profile at the membrane position in a simulation with $\nu_p = 1.0$ km/s, $\tau_s = 3$ ps and a nanobubble with a diameter, $D = 20$ nm).

But the impulse created by the nanojet itself is smaller, and the impact area on the membrane is also smaller. Another difference between the two cases is that the bigger bubble collapse takes a longer time and nanojet hits the membrane after the shock wave completely passes it, whereas in the smaller bubble case the nanojet collapse on the membrane occurs immediately after the shock wave passed. This difference can be clearly seen from the corresponding pressure profiles: separate peaks are seen in Figure 6 for the bigger bubble, whereas for the smaller bubble (Figure 11) the nanojet pressure peak is overlapping with the shock wave pressure peak. The normal pressure distribution along the x and y axes of the membrane is similar to the distribution observed in case of the bigger bubble, as expected, but the impact of the nanojet pressure is focused on a smaller area of the membrane. This results in the formation of a smaller pore in the membrane. The 2-d pressure maps and snapshots of the membrane at various times are given in Figures S10 and S11 of the Supporting Information.

Spontaneous Nanobubble Collapse (without Shock Wave). The nanobubble can collapse spontaneously. If the surrounding is symmetrical, the bubble collapse will be also symmetrical, but if the bubble is located next to a membrane the collapse is asymmetrical and it may produce membrane damage. To see what happens during the spontaneous collapse

of the nanobubble, we simulated a system containing a membrane and a nanobubble with $D = 60$ nm. The time step of 20 fs was used in these simulations. The results depended on the ensemble used. In case of the constant pressure and temperature (NPT) ensemble, the bubble collapsed completely at 2.2 ns. Since the membrane is located very closely to the edge of the bubble (~ 3 nm), the bilayer part closest to the bubble bended toward the center of the bubble and membrane became curved, although no pore formation in the membrane was observed. After the completion of the bubble collapse, the bilayer recovered to its original form at 30 ns. Some snapshots of the membrane at various simulations are provided in Supporting Information, Figure S12. When we performed the simulation in the NPzAT ensemble, where the lateral area of the membrane was kept constant, a complete bubble collapse occurred at about 4.6 ns, which is twice the time interval needed to observe the collapse in the NPT ensemble. We observed that the membrane was less curved in this case, compared to the one from the simulation performed using the NPT ensemble, and that it fully recovered at about 25 ns. Again no pore formation was observed. Thus, a spontaneous bubble collapse next to the membrane did not produce damage to membrane in the form of a pore.

■ DISCUSSIONS AND SUMMARY

To understand the role of cavitation effect in the presence of nanobubbles, we performed simulations on systems containing model membranes and considered what happened when shock waves impinged on them, in absence or presence of the bubbles. As we observed, in the absence of a bubble a shock wave impulse of a rather small value of around 18 mPa s does not damage the membrane. We study cases with a small value of impulse, because we are interested in the possible damage to cell membranes produced during mild traumatic brain injury. We observed that the membrane was compressed for a short duration, but recovered within a short time. Our results are consistent with earlier simulations by Koshiyama et.al³ that did not see creation of pores in membranes, even when a shock wave had an impulse of 50 mPa s, but are in contradiction with the conclusion from the recently reported in the literature simulation⁸ that an impulse bigger or equal to 0.45 mPa s damages the bilayer to an unrecoverable state. It should be noted that the system considered in that study was very small and a different methodology was applied for shock wave generation.

The presence of a nanobubble next to a membrane changes the result quite dramatically. In this case, once the shock wave impinges on the nanobubble, it induces its collapse, which results in the formation of a nanojet directed toward the membrane. The nanojet impinges on the membrane and makes a pore in it, even if the impulse transferred to a membrane is smaller than the one in pure shock wave case. Why is the membrane not damaged by a shock wave that hit the system when no bubble is present, but a pore is formed when a bubble is present, although the pressure impulse in the system with no bubble can be larger than in the system with a bubble? To understand this we calculated pressure distributions along the plane of the membrane and found them to be very informative. Pressure distribution maps revealed that when the shock wave passes over the membrane it creates a negative pressure region on the membrane surface. At the same time due to the bubble collapse a positive pressure region appears at the membrane center. For example, in the case when $v_p = 1.0$ km/s, and $\tau_s = 3$

ps, the difference between positive and negative pressures is quite large, around 100 MPa. This unequal distribution of pressures causes a disbalance of stresses acting in different direction on the membrane, resulting in pore formation. Since it is the pressure distribution that is responsible for the membrane damage, we cannot use the impulse delivered to the membrane (eq 1) as the quantitative parameter that is correlated to the degree of the membrane damage. One can consider the total impulse that includes the impulse after the first shock and the consequent impulse due to pressure rise after the jet reaches the membrane as a factor in measuring the disruption, but more work needs to be done to establish quantitative criteria that predict membrane damage.

We already mentioned that a choice of parameters τ_s and v_p plays an important role. In fact, the unequal distribution of pressure on the membrane becomes much more pronounced if the piston is stopped at 5 ps instead of 3 ps. When $\tau_s = 5$ ps, the difference between the highest and lowest pressures is larger than 300 MPa, three times the difference observed in case when $\tau_s = 3$ ps. When we reduced v_p from 1.0 km/s to 0.5 km/s the maximum difference between the high and low pressure regions was not larger than 40 MPa and we did not observe a pore formation in the membrane. Interestingly, when the piston was stopped at 10 ps, (but v_p was still 0.5 km/s), the total impulse and the pressure distribution at the membrane was similar to that in the case when $v_p = 1.0$ km/s and $\tau_s = 3$ ps and similar pores in membrane were formed.

In summary, while the shock wave impinging on a lipid bilayer membrane may produce damage to it, the presence of nanobubbles located next to bilayer that are hit by the shock wave substantially increases the damage done to membranes. Since biological membranes represent much more complex systems than membranes containing just one lipid component, considered here, the next step in simulations is to study how the complexity of membranes influence the cavitation effect. Particularly interesting is to study how the proteins, such as channels behave when cavitation of bubbles occur.

■ ASSOCIATED CONTENT

Supporting Information

Snapshots of the bilayer membrane at various times of the simulations, 2-dimensional pressure maps, and 2d water density maps and the corresponding snapshots. The Supporting Information is available free of charge on the ACS Publications website at DOI: 10.1021/acs.jpcb.5b02218.

■ AUTHOR INFORMATION

Corresponding Author

*(M.L.B.) E-mail: maxb@unc.edu.

Notes

The authors declare no competing financial interest.

■ ACKNOWLEDGMENTS

The support by Grant N00014-14-1-0241 from the Office of Naval Research is gratefully acknowledged. We are thankful to Lawrence Livermore National Laboratory for providing computing facilities.

■ REFERENCES

- (1) Choubey, A.; Vedadi, M.; Nomura, K.; Kalia, R. K.; Nakano, A.; Vashishta, P. Poration of Lipid Bilayers by Shock-Induced Nanobubble Collapse. *Appl. Phys. Lett.* 2011, 98, 023701.

- (2) Kodama, T.; Hamblin, M. R.; Doukas, A. G. Cytoplasmic Molecular Delivery with Shock Waves: Importance of Impulse. *Biophys. J.* **2000**, *79*, 1821–1832.
- (3) Koshiyama, K.; Kodama, T.; Yano, T.; Fujikawa, S. Structural Change in Lipid Bilayers and Water Penetration Induced by Shock Waves: Molecular Dynamics Simulations. *Biophys. J.* **2006**, *91*, 2198–2205.
- (4) Mediavilla Varas, J.; Philippens, M.; Meijer, S. R.; van den Berg, A. C.; Sibma, P. C.; van Bree, J. L. M. J.; de Vries, D. V. W. M. Physics of IED Blast Shock Tube Simulations for mTBI Research. *Front. Neurol.* **2011**, *2*, 58.
- (5) Santo, K. P.; Berkowitz, M. L. Shock Wave Interaction with a Phospholipid Membrane: Coarse-Grained Computer Simulations. *J. Chem. Phys.* **2014**, *140*, 054906.
- (6) Steinhauser, M. O.; Schmidt, M. Destruction of Cancer Cells by Laser-Induced Shock Waves: Recent Developments in Experimental Treatments and Multiscale Computer Simulations. *Soft Matter* **2014**, *10*, 4778–4788.
- (7) Nakagawa, A.; Manley, G. T.; Gean, A. D.; Ohtani, K.; Armonda, R.; Tsukamoto, A.; Yamamoto, H.; Takayama, K.; Tominaga, T. Mechanisms of Primary Blast-Induced Traumatic Brain Injury: Insights from Shock-Wave Research. *J. Neurotrauma* **2011**, *28*, 1101–1119.
- (8) Espinosa, S.; Asproulis, N.; Drikakis, D. Chemotherapy Efficiency Increase via Shock Wave Interaction with Biological Membranes: A Molecular Dynamics Study. *Microfluid. Nanofluidics* **2013**, *16*, 613–622.
- (9) Afadzi, M.; Strand, S. P.; Nilssen, E. A.; Måsøy, S.-E.; Johansen, T. F.; Hansen, R.; Angelsen, B. A.; de L Davies, C. Mechanisms of the Ultrasound-Mediated Intracellular Delivery of Liposomes and Dextrans. *IEEE Trans. Ultrason. Ferroelectr. Freq. Control* **2013**, *60*, 21–33.
- (10) Ahmed, S. E.; Martins, A. M.; Husseini, G. A. The Use of Ultrasound to Release Chemotherapeutic Drugs from Micelles and Liposomes. *J. Drug Target.* **2015**, *23*, 16–42.
- (11) Arun, P.; Abu-Taleb, R.; Oguntayo, S.; Tanaka, M.; Wang, Y.; Valiyaveettil, M.; Long, J. B.; Zhang, Y.; Nambiar, M. P. Distinct Patterns of Expression of Traumatic Brain Injury Biomarkers after Blast Exposure: Role of Compromised Cell Membrane Integrity. *Neurosci. Lett.* **2013**, *552*, 87–91.
- (12) De Cock, I.; Zagato, E.; Braeckmans, K.; Luan, Y.; de Jong, N.; De Smedt, S. C.; Lentacker, I. Ultrasound and Microbubble Mediated Drug Delivery: Acoustic Pressure as Determinant for Uptake via Membrane Pores or Endocytosis. *J. Controlled Release* **2015**, *197*, 20–28.
- (13) Deng, C. X.; Sieling, F.; Pan, H.; Cui, J. Ultrasound-Induced Cell Membrane Porosity. *Ultrasound Med. Biol.* **2004**, *30*, 519–526.
- (14) Gambihler, S.; Delius, M. Transient Increase in Membrane Permeability of L1210 Cells upon Exposure to Lithotripter Shock Waves in Vitro. *Naturwissenschaften* **1992**, *79*, 328–329.
- (15) Horie, S.; Watanabe, Y.; Chen, R.; Mori, S.; Matsumura, Y.; Kodama, T. Development of Localized Gene Delivery Using a Dual-Intensity Ultrasound System in the Bladder. *Ultrasound Med. Biol.* **2010**, *36*, 1867–1875.
- (16) Husseini, G. A.; Pitt, W. G.; Martins, A. M. Ultrasonically Triggered Drug Delivery: Breaking the Barrier. *Colloids Surf. B: Biointerfaces* **2014**, *123*, 364–386.
- (17) Ng, K.; Liu, Y. Therapeutic Ultrasound: Its Application in Drug Delivery. *Med. Res. Rev.* **2002**, *22*, 204–223.
- (18) Panzer, M. B.; Matthews, K. A.; Yu, A. W.; Morrison, B.; Meaney, D. F.; Bass, C. R. A Multiscale Approach to Blast Neurotrauma Modeling: Part I - Development of Novel Test Devices for in Vivo and in Vitro Blast Injury Models. *Front. Neurol.* **2012**, *3*, 46.
- (19) Ravin, R.; Blank, P. S.; Steinkamp, A.; Rappaport, S. M.; Ravin, N.; Bezrukov, L.; Guerrero-Cazares, H.; Quinones-Hinojosa, A.; Bezrukova, S. M.; Zimmerberg, J. Shear Forces during Blast, Not Abrupt Changes in Pressure Alone, Generate Calcium Activity in Human Brain Cells. *PLoS One* **2012**, *7*, e39421.
- (20) Rosenfeld, J. V.; McFarlane, A. C.; Bragge, P.; Armonda, R. A.; Grimes, J. B.; Ling, G. S. Blast-Related Traumatic Brain Injury. *Lancet. Neurol.* **2013**, *12*, 882–893.
- (21) Sliozberg, Y.; Chantawansri, T. Damage in Spherical Cellular Membrane Generated by the Shock Waves: Coarse-Grained Molecular Dynamics Simulation of Lipid Vesicle. *J. Chem. Phys.* **2014**, *141*, 184904.
- (22) Hernot, S.; Klibanov, A. L. Microbubbles in Ultrasound-Triggered Drug and Gene Delivery. *Adv. Drug Delivery Rev.* **2008**, *60*, 1153–1166.
- (23) Postema, M.; van Wamel, A.; Lancée, C. T.; de Jong, N. Ultrasound-Induced Encapsulated Microbubble Phenomena. *Ultrasound Med. Biol.* **2004**, *30*, 827–840.
- (24) Prentice, P.; Cuschieri, A.; Dholakia, K.; Prausnitz, M.; Campbell, P. Membrane Disruption by Optically Controlled Microbubble Cavitation. *Nat. Phys.* **2005**, *1*, 107–110.
- (25) Kobayashi, K.; Kodama, T.; Takahira, H. Shock Wave-Bubble Interaction near Soft and Rigid Boundaries during Lithotripsy: Numerical Analysis by the Improved Ghost Fluid Method. *Phys. Med. Biol.* **2011**, *56*, 6421–6440.
- (26) Lentacker, I.; De Cock, I.; Deckers, R.; De Smedt, S. C.; Moonen, C. T. W. Understanding Ultrasound Induced Sonoporation: Definitions and Underlying Mechanisms. *Adv. Drug Delivery Rev.* **2014**, *72*, 49–64.
- (27) Qiu, Y.; Luo, Y.; Zhang, Y.; Cui, W.; Zhang, D.; Wu, J.; Zhang, J.; Tu, J. The Correlation between Acoustic Cavitation and Sonoporation Involved in Ultrasound-Mediated DNA Transfection with Polyethylenimine (PEI) in Vitro. *J. Controlled Release* **2010**, *145*, 40–48.
- (28) Ohl, C.-D.; Arora, M.; Ikink, R.; de Jong, N.; Versluis, M.; Delius, M.; Lohse, D. Sonoporation from Jetting Cavitation Bubbles. *Biophys. J.* **2006**, *91*, 4285–4295.
- (29) Kodama, T.; Tomita, Y.; Watanabe, Y.; Koshiyama, K.; Yano, T.; Fujikawa, S. Cavitation Bubbles Mediated Molecular Delivery During Sonoporation. *J. Biomech. Sci. Eng.* **2009**, *4*, 124–140.
- (30) Santo, K. P.; Berkowitz, M. L. Shock Wave Induced Collapse of Arrays of Nanobubbles Located Next to a Lipid Membrane: Coarse-Grained Computer Simulations. *J. Phys. Chem. B* **2014**, DOI: 10.1021/jp505720d.
- (31) Attard, P. The Stability of Nanobubbles. *Eur. Phys. J. Spec. Top.* **2013**, *1*–22.
- (32) Borkent, B.; Dammer, S.; Schönher, H.; Vancso, G.; Lohse, D. Superstability of Surface Nanobubbles. *Phys. Rev. Lett.* **2007**, *98*, 204502.
- (33) Craig, V. S. J. Very Small Bubbles at Surfaces—the Nanobubble Puzzle. *Soft Matter* **2011**, *7*, 40.
- (34) Lukianova-Hleb, E. Y.; Ren, X.; Sawant, R. R.; Wu, X.; Torchilin, V. P.; Lapotko, D. O. On-Demand Intracellular Amplification of Chemoradiation with Cancer-Specific Plasmonic Nanobubbles. *Nat. Med.* **2014**, *20*, 778–784.
- (35) Weijns, J.; Lohse, D. Why Surface Nanobubbles Live for Hours. *Phys. Rev. Lett.* **2013**, *110*, 054501.
- (36) Attard, P.; Moody, M. P.; Tyrrell, J. W. G. Nanobubbles: The Big Picture. *Phys. A Stat. Mech. Its Appl.* **2002**, *314*, 696–705.
- (37) Hess, B.; Kutzner, C.; van der Spoel, D.; Lindahl, E. GROMACS 4: Algorithms for Highly Efficient, Load-Balanced, and Scalable Molecular Simulation. *J. Chem. Theory Comput.* **2008**, *4*, 435–447.
- (38) Van Der Spoel, D.; Lindahl, E.; Hess, B.; Groenhof, G.; Mark, A. E.; Berendsen, H. J. C. GROMACS: Fast, Flexible, and Free. *J. Comput. Chem.* **2005**, *26*, 1701–1718.
- (39) Lindahl, E.; Hess, B.; Spoel, D. van der. GROMACS 3.0: A Package for Molecular Simulation and Trajectory Analysis. *Mol. Model. Annu.* **2001**, *7*, 306–317.
- (40) Berendsen, H. J. C.; van der Spoel, D.; van Drunen, R. GROMACS: A Message-Passing Parallel Molecular Dynamics Implementation. *Comput. Phys. Commun.* **1995**, *91*, 43–56.
- (41) Ollila, O.; Risselada, H.; Louhivuori, M.; Lindahl, E.; Vattulainen, I.; Marrink, S. 3D Pressure Field in Lipid Membranes and Membrane-Protein Complexes. *Phys. Rev. Lett.* **2009**, *102*, 078101.

- (42) Marrink, S. J.; Risselada, H. J.; Yefimov, S.; Tieleman, D. P.; de Vries, A. H. The MARTINI Force Field: Coarse Grained Model for Biomolecular Simulations. *J. Phys. Chem. B* **2007**, *111*, 7812–7824.
- (43) Marrink, S. J.; de Vries, A. H.; Mark, A. E. Coarse Grained Model for Semiquantitative Lipid Simulations. *J. Phys. Chem. B* **2004**, *108*, 750–760.
- (44) De Jong, D. H.; Singh, G.; Bennett, W. F. D.; Arnarez, C.; Wassenaar, T. A.; Schäfer, L. V.; Periole, X.; Tieleman, D. P.; Marrink, S. J. Improved Parameters for the Martini Coarse-Grained Protein Force Field. *J. Chem. Theory Comput.* **2013**, *9*, 687–697.
- (45) Monticelli, L.; Kandasamy, S. K.; Periole, X.; Larson, R. G.; Tieleman, D. P.; Marrink, S.-J. The MARTINI Coarse-Grained Force Field: Extension to Proteins. *J. Chem. Theory Comput.* **2008**, *4*, 819–834.
- (46) Berendsen, H. J. C.; Postma, J. P. M.; van Gunsteren, W. F.; DiNola, A.; Haak, J. R. Molecular Dynamics with Coupling to an External Bath. *J. Chem. Phys.* **1984**, *81*, 3684.
- (47) Vedadi, M.; Choubey, A.; Nomura, K.; Kalia, R. K.; Nakano, A.; Vashishta, P.; van Duin, A. C. T. Structure and Dynamics of Shock-Induced Nanobubble Collapse in Water. *Phys. Rev. Lett.* **2010**, *105*, 014503.
- (48) Nomura, K.-I.; Kalia, R. K.; Nakano, A.; Vashishta, P.; van Duin, A. C. T.; Goddard, W. A. Dynamic Transition in the Structure of an Energetic Crystal during Chemical Reactions at Shock Front prior to Detonation. *Phys. Rev. Lett.* **2007**, *99*, 148303.
- (49) Humphrey, W.; Dalke, A.; Schulten, K. VMD: Visual Molecular Dynamics. *J. Mol. Graph.* **1996**, *14*, 33–38.